Mon. Not. R. Astron. Soc. **000**, 000–000 (0000) Printed 20 January 2013 (MN LaTeX style file v2.2)

Minimal HCN emission from Molecular Clouds in M33

Erik Rosolowsky,[1], Jaime E. Pineda,[2,3], Yu Gao[4]
[1] *University of British Columbia Okanagan, 3333 University Way, Kelowna BC V1V 1V7 Canada*
[2] *Harvard-Smithsonian Center for Astrophysics, 60 Garden St., MS-10, Cambridge, MA 02138, USA*
[3] *Jodrell Bank Centre for Astrophysics, School of Physics and Astronomy, University of Manchester, Oxford Road, Manchester, M13 9PL, UK*
[4] *Purple Mountain Observatory, Chinese Academy of Sciences (CAS), 2 West Beijing Road, Nanjing 210008, China*

arXiv:1104.3935v1 [astro-ph.GA] 20 Apr 2011

20 January 2013

ABSTRACT

Since HCN emission has been shown to be a linear tracer of ongoing star formation activity, we have searched for HCN ($J = 1 \rightarrow 0$) emission from known GMCs in the nearby galaxy M33. No significant HCN emission has been found along any of the lines of sight. We find two lines of sight where CO-to-HCN integrated intensity ratios up to 280, nearly a factor of 6 above what is found in comparable regions of the Milky Way. Star formation tracers suggest that the HCN-to-star formation rate ratio ($L_{\mathrm{HCN}}/\dot{M}_\star$) is a factor of six lower than what is observed in the Milky Way (on average) and local extragalactic systems. Simple chemical models accounting for the sub-solar N/O ratio suggest that depletion cannot account for the high CO-to-HCN ratios. Given HCN formation requires high extinction ($A_V > 4$), low metallicity may yield reduced dust shielding and thus a high CO/HCN ratio. The turbulence and structure of GMCs in M33 are comparable to those found in other systems, so the differences are unlikely to result from different GMC properties. Since lower CO-to-HCN ratios are associated with the highest rates of star formation, we attribute the deficits in part to evolutionary effects within GMCs.

1 INTRODUCTION

All local star formation is invariably associated with molecular gas, but recent studies have clarified that star formation is associated exclusively with *dense* ($n > 10^5$ cm^{-3}) molecular gas from the scales of cores (Lada 1992; Wu et al. 2005, 2010) to galaxies (Gao & Solomon 2004; Gao et al. 2007). Most of the gas typically observed in studies of molecular clouds on large scales (> 10 pc) is found at lower densities ($n \sim 10^2$ cm^{-3}), but dense gas studies suggest that the low-density gas is not directly involved in the star formation process. This clarification is particularly important for studies of the galaxy-scale star formation since the molecular gas content of a external galaxy is usually traced with emission from low-J transitions of ^{12}CO, which are excited in the low density molecular gas which traces the bulk of material found in molecular clouds (e.g., Pineda et al. 2008).

Relatively few large-scale studies of the dense molecular gas content of galaxies have been conducted. The majority of mass in the dense gas is found as molecular hydrogen, which emits no radiation at the densities and temperatures typical of star forming clouds. Observations rely on emission from dense gas tracers, which are excited to emission only at the high densities. Typical tracers include line emission from HCN, N_2H^+, NH_3 and HCO^+, all of which have critical densities of order 10^5 cm^{-3}. While the relative merits of these tracers have been compared (Shirley et al. 2008), all seem to produce similar results: the dense gas that they trace is linearly related to the star formation rate

$$\frac{\Sigma_{\mathrm{SFR}}}{M_\odot\ \mathrm{yr}^{-1}\ \mathrm{pc}^{-2}} \propto \left(\frac{\Sigma_{\mathrm{dense}}}{M_\odot\ \mathrm{pc}^{-2}}\right)^{1.0}. \tag{1}$$

These results even seem to hold for high-redshift systems (Gao et al. 2007).

Even though low-density molecular gas does not participate directly in star formation, there has been extensive work demonstrating that low-density gas is indeed related to star formation on a galactic scale. While originally demonstrated for galaxies as a whole (Kennicutt 1998), recent work has shown the relationship holds for molecular gas on scales of > 500 pc (Wong & Blitz 2002; Heyer et al. 2004; Kennicutt 2007; Bigiel et al. 2008). These studies find $\Sigma_{\mathrm{SFR}} \propto \Sigma_{\mathrm{H2}}^{\alpha}$, where $\alpha = 1.0$ to 1.4 depending on analysis methods used. The apparent difference in star formation relationships for low- and high-density molecular gas can likely be attributed to changing dense-gas fractions in a galaxy's ISM (Gao & Solomon 2004). Some authors argue that the index of the star formation law can be predicted from the average density of the medium compared to the critical density of tracer in question (Krumholz & Thompson 2007; Narayanan et al. 2008), with additional considerations regarding excitation of higher levels. Even with these considerations, the ($1 \rightarrow 0$) line of HCN should provide a linear tracer of dense gas mass and an index of unity on the star formation law. Thus, a compelling model emerges where the star formation process in a galaxy can be decoupled into two steps: the formation of dense gas within a molecular cloud and the subsequent formation of stars in that high-density gas *at a constant rate* (or a constant fraction per free-fall

© 0000 RAS

time, Krumholz & Thompson 2007). The apparent changes in the star formation efficiency ($\Sigma_{\rm H2}/\Sigma_{\rm SFR}$) can then be attributed to change in the molecular cloud properties in galaxies, specifically the fraction of the cloud found at high density.

Comparing the CO and HCN emission from individual molecular clouds can test whether there is significant change in the fraction of dense gas within individual molecular clouds. Some studies have been undertaken for Milky Way molecular clouds (e.g., Helfer & Blitz 1997), suggesting that dense gas fraction of molecular gas does indeed change as a function of distance from the centre of the Galaxy. The study of Brouillet et al. (2005) examined the CO-to-HCN intensity ratio across the disk of the massive galaxy M31, finding a radial decline in the ratio with a maximum ratio of $I_{\rm CO}/I_{\rm HCN} = 125$. It remains unclear based on these results the degree to which the changes in the CO-to-HCN ratio result from changes in molecular clouds properties or whether the relationship between the tracers and the underlying H_2 is changing.

The nearby galaxy M33 has been noted to exhibit a particularly high star formation efficiency (Heyer et al. 2004; Rosolowsky et al. 2007; Gardan et al. 2007) based on observations of CO emission. In the context of the above star formation model, this would imply that the dense gas fractions of the molecular clouds in M33 would be higher than that of the typical galaxy. Other circumstances may explain the high star formation efficiency of the galaxy since M33 is distinct from M31 and the Milky Way in two ways. First, it has a significantly lower metallicty outside the central region ($12 + \log({\rm O/H}) = 8.4$ Magrini et al. 2007; Rosolowsky & Simon 2008); and second, it has a significantly lower mass ($M_{\rm M33} \sim M_{\rm MW}/10$). Given its proximity and previous study it is possible to assess how tracers of high- and low-density molecular gas relate on the scale on individual giant molecular clouds. To this end, we have undertaken observations of CO and HCN toward giant molecular clouds (GMCs) in M33 using the IRAM 30-m telescope.

2 MOLECULAR LINE OBSERVATIONS

We observed the positions of four Giant Molecular Clouds (GMCs) in M33 using the IRAM 30-m telescope located in Pico Veleta, Spain. The observations were carried out from 16th to 20th of July 2007. HCN ($1 \rightarrow 0$) and ^{13}CO ($2 \rightarrow 1$) were observed simultaneously with the VESPA back-end in the 80 kHz resolution mode. The same configuration was used to observe ^{12}CO ($1 \rightarrow 0$) and ^{12}CO ($2 \rightarrow 1$) simultaneously. All the observations were taken in position-switching mode. Weather conditions were good for summer observations and pointing observations imply a pointing accuracy of $< 5''$. Of note, this accuracy is small compared to the 89 GHz beam (HCN($1 \rightarrow 0$)) but is more significant when compared to the 230 GHz beam (^{12}CO($2 \rightarrow 1$)). Opacity and system temperature for each of the transitions is given in Table 1 and integration time (t_{int}) and per-channel rms (σ) for the HCN/^{13}CO configuration is given in Table 2.

Conversion from the measured T_A^* to $T_{\rm mb}$ is carried out as $T_{\rm mb} = T_A^* F_{eff}/B_{eff}$. The forward ($F_{eff}$) and beam ($B_{eff}$) efficiencies were determined by measurements made by observatory staff. A summary of the observation's parameters is presented in Table 1 and the spectra are shown in Figure 2. The data were reduced using the CLASS90 software.

Table 1. Observational parameters

Line	Freq. (GHz)	F_{eff}	B_{eff}	$\theta_{\rm FWHM}$ (arcsec)	$\langle T_{sys} \rangle$ (K)	$\langle \tau \rangle$
^{12}CO($1 \rightarrow 0$)	115.2712	0.95	0.75	22	250	0.28
^{12}CO($2 \rightarrow 1$)	230.538	0.91	0.52	11	250	0.11
^{13}CO($2 \rightarrow 1$)	220.3986	0.91	0.57	12	250	0.11
HCN($1 \rightarrow 0$)	88.63160	0.95	0.78	28	110	0.05

We selected four targets from the GMC catalog of Rosolowsky et al. (2007) based on strong CO emission with a range of star formation properties. We summarize the observations of the GMCs in Table 2 and their locations are shown in Figure 1. We did not detect HCN ($1 \rightarrow 0$) emission in at least two of the four lines of sight. M33GMC 1, the pointing closest to the center of the galaxy, shows a modest detection at a low level, as does M33GMC 76. For each line-of-sight, we measure the integrated intensity $I_{\rm HCN} = \sum T_{\rm mb} \delta V$ where δV is the channel width, where the sum is carried out over the expected velocity range of the HCN line assuming it has the same intrinsic line width as the CO line but accounting for hyperfine structure. We establish a 3σ upper limit as

$$I_{\rm HCN} < 3\sigma_{\rm HCN}\Delta V \left[(1 - N/N_{tot})\right]^{-0.5}, \qquad (2)$$

where $\sigma_{\rm HCN}$ is the rms noise fluctuation in the spectrum, ΔV is the velocity width of the HCN line, N is the number of channels across ΔV and N_{tot} is the number of channels in the entire spectrum (Matthews & Gao 2001).

We further process these observations to place them on a common standard and supplement the results with a significant amount of ancillary data, the results of which are given in Table 2. The integrated intensities are given as I_{10}, I_{21} and I_{13} for the ^{12}CO($1 \rightarrow 0$), ^{12}CO($2 \rightarrow 1$), and ^{13}CO($1 \rightarrow 0$) lines respectively. For comparison to other work, molecular line intensities are scaled to luminosities for the lines by multiplying by the projected area of the beam for that tracer.

For a rigourous comparison of line intensities, all data must be sampled with the same resolution. To properly estimate the CO-to-HCN ratio, we convolved the fully sampled, high resolution ^{12}CO($1 \rightarrow 0$) map of Rosolowsky et al. (2007) to the $28''$ resolution of the IRAM beam at 89 GHz and sampled the map at the observed positions. These values are reported as $I_{10,\rm R07}$ and $I_{10,\rm convol}$ in Table 2 for pre- and post-convolution respectively. We checked the relative calibrations of the map by convolving the same map to the $22''$ resolution of the IRAM ^{12}CO ($1 \rightarrow 0$) observations and comparing the observed and predicted integrated intensities finding them consistent to the 10% level expected from the amplitude calibrations of the two maps.

We supplement the molecular line data with infrared and optical band observations which are indicators of the star formation rate. To derive the star formation rate, we use combined Hα+24 μm emission derived from data from the Local Group Survey (Massey et al. 2007) and Spitzer/MIPS observations of the galaxy (Polomski et al. 2006) respectively. A continuum subtracted Hα image was generated

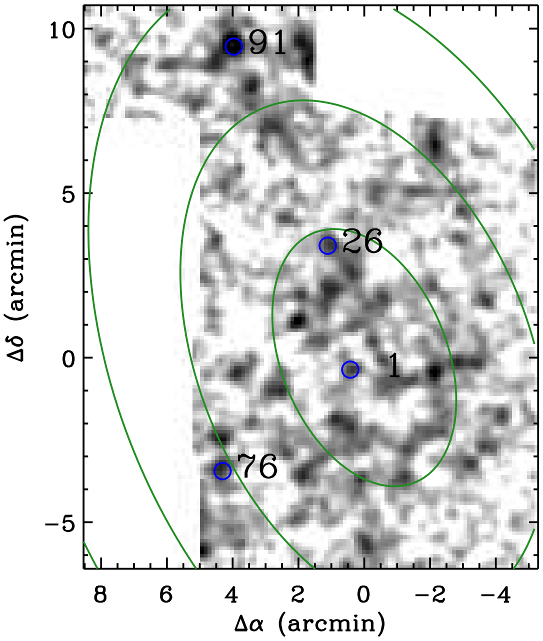

Figure 1. Locations of the four IRAM lines of sight overlaid on an integrated intensity of CO ($1 \to 0$) emission. Three contours of constant galactocentric radius are indicated with ellipses representing $R_{\mathrm{kpc}} = 1, 2$ and 3 kpc.

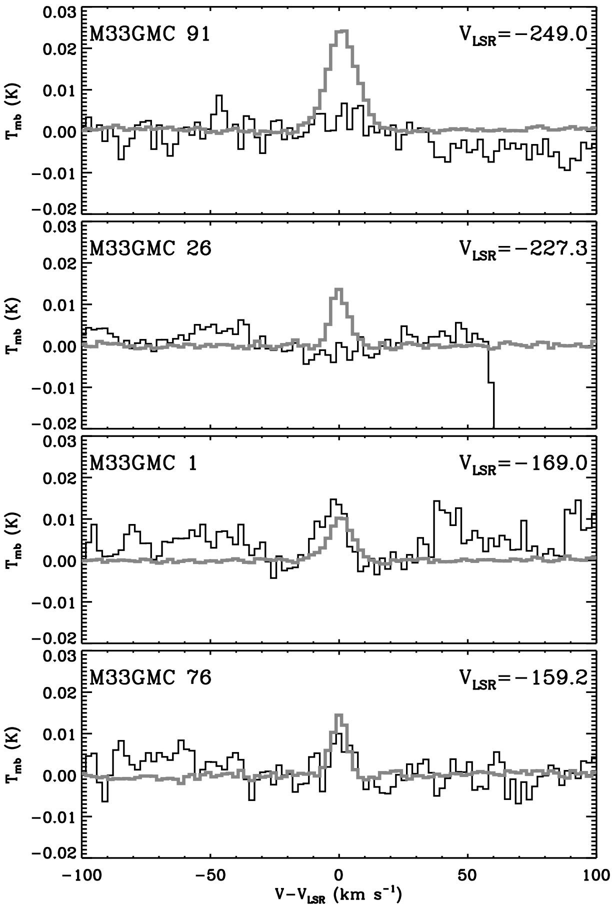

Figure 2. IRAM 30-m observations of HCN ($1 \to 0$) and ^{12}CO ($1 \to 0$) shown as black and gray lines respectively. The CO spectra have been scaled down by a factor of 100 for ease of comparison with the HCN data. The spectra have been Hanning smoothed and decimated to 2 km s^{-1} resolution.

by subtracting off an optimally scaled R band image from the Hα filter and scaling to photometric units based on Massey et al. (2007). The MIPS data were from the calibrated images of Hinz et al. (2004) and Tabatabaei et al. (2007). Each image was convolved to the 28″ IRAM beam and sampled at the locations of the IRAM pointings. The local star formation was established using the prescription of Kennicutt et al. (2007):

$$\dot{M}_\star\ (M_\odot\ \mathrm{yr}^{-1}) = 7.9 \times 10^{-42}\,[L_{\mathrm{H}\alpha} + 0.039\ \nu_{24} L_\nu(24)] \qquad (3)$$

where luminosities are measured in erg s^{-1} and refer to the Hα line and the Spitzer 24-micron band respectively.

We also estimate the total infrared luminosity using all three MIPS bands following Dale & Helou (2002).

$$L_{\mathrm{TIR}} = w_1 \nu L_\nu(24\,\mu m) + w_2 \nu L_\nu(70\,\mu m) + w_3 \nu L_\nu(160\,\mu m), \quad (4)$$

where $w_1 = 1.559$, $w_2 = 0.7686$ and $w_3 = 1.6381$. The MIPS 160 μm band image is sampled without convolution since the resolution is larger than the HCN: 40″ vs. 28″, resulting in an additional uncertainty in L_{TIR} of 15%. We also estimate the local pressure in the galaxy using the estimator presented by Blitz & Rosolowsky (2006) and we report these values of P/k in Table 2. The total mass of the observed GMC as determined from the high-resolution map (R07) is given as M_{CO}. The “Comparisons” section of the table highlights the most important results as discussed in §3 below.

3 ANALYSIS AND RESULTS

The minimal HCN emission from the galaxy was unexpected given the predicted ratios of $I_{\mathrm{CO}}/I_{\mathrm{HCN}}$ from other studies. For normal galaxies, Gao & Solomon (2004) find $L_{\mathrm{CO}}/L_{\mathrm{HCN}} = 25$ with $\sim 50\%$ scatter. For GMCs in the disk in the Milky Way, Helfer & Blitz (1997) find $I_{\mathrm{CO}}/I_{\mathrm{HCN}} = 40 \pm 10$ but the ratio decreases for clouds in the bulge of the galaxy to 12. For comparison, we find two sources (M33GMC 91 and 26) with a dense gas ratio > 280 and the remaining two sources have a ratio below that of the Milky Way disk. We conclude that the HCN emission from M33 GMCs, relative to their CO, is a factor of 2 to 7 lower than similar clouds in the disk of the Milky Way and other galaxies.

The lack of HCN emission becomes even more remarkable when the results are compared with expectations based on the measured star formation rate of M33. Previous work by Wu et al. (2005) suggests that the rate of ongoing star formation is linearly related to the luminosity of HCN ($1 \to 0$):

$$\dot{M}_\star\ (M_\odot\ \mathrm{yr}^{-1}) = 1.4 \times 10^{-7} L_{\mathrm{HCN}}\ (\mathrm{K\ km\ s^{-1}\ pc^2}). \qquad (5)$$

We estimate the amount of HCN emission that would be predicted based on the apparent star formation at each of

Table 2. M33 GMCs observed

Property	M33GMC 91	M33GMC 26	M33GMC 1	M33GMC 76
α_{2000}	01 34 09.2	01 33 55.8	01 33 52.4	01 34 10.7
δ_{2000}	+30 49 06	+30 43 02	+30 39 18	+30 36 15
V_{LSR} (km s^{-1})	−249.0	−227.3	−169.0	−159.2
t_{int} (min)	246	217	244	213
σ (mK)	7.1	3.1	5.6	5.5
I_{10} (K km s^{-1})	21.6	6.9	7.2	6.5
I_{21} (K km s^{-1})	25.2	7.0	15.5	9.6
I_{13} (K km s^{-1})	1.4	0.3	1.8	1.6
$I_{\rm HCN}$ (K km s^{-1})	< 0.053	< 0.027	~ 0.12	~ 0.059
L_{10} (10^3 K km s^{-1} pc^2)^a	150	53	47	59
$L_{\rm HCN}$ (10^3 K km s^{-1} pc^2)^a	< 0.75	< 0.40	~ 1.90	~ 0.94
Ancillary Data				
$I_{10,\rm R07}$ (K km s^{-1})	29.0	12	11	11
$I_{10,\rm convol}$ (K km s^{-1})	13.1	5.0	4.4	5.2
$L_{\rm H\alpha}$ (10^3 $L_\odot$)^a	1.4	2.9	34	10
$\nu_{24}L_\nu(24)$ (10^3 $L_\odot$)^a	61	78	470	250
$L_{\rm TIR}$ (10^6 $L_\odot$)^a	1.4	1.5	6.0	3.0
$\Sigma_{\rm SFR}$ ($M_\odot$ Gyr^{-1} pc^{-2})	8	12	110	43
P/k (10^4 K cm^{-3})	1.6	1.6	2.4	1.2
$M_{\rm CO}$ (10^5 $M_\odot$)	11.1	6.3	3.1	3.5
Comparisons				
$I_{\rm HCN}$ (K km s^{-1})	< 0.053	< 0.027	~ 0.12	~ 0.059
$I_{{\rm HCN},pred}$ (K km s^{-1})	0.060	0.090	0.79	0.310
$I_{10,\rm convol}/I_{\rm HCN}$	> 280	> 190	~ 37	~ 91
$L_{\rm TIR}/L_{\rm HCN}{}^b$	> 2000	> 4200	~ 3300	~ 3300
$L_{\rm TIR}/L_{\rm CO}{}^b$	7.2	22	92	38

[a] For conversion between intrinsic properties and quantities derived from surface brightness, note that the 28″ IRAM beam subtends 1.5×10^4 pc^2 at the 840 kpc distance of M33 (Freedman et al. 2001).

[b] $L_\odot$/(K km s^{-1} pc^2)

our pointing locations in M33. Using the star formation rate estimates presented in Table 2, we use Eq. 5 to predict the intensity of HCN emission expected from the ongoing star formation ($I_{{\rm HCN},pred}$ in Table 2). We find the predicted HCN emission is a factor of 1.1 to 6.6 higher than the observed values or upper limits. The discrepancy may result, in part, from the inclusion of Hα in the star formation indicator vs. the infrared-only data used in Equation 5.

The ^{12}CO ($2 \rightarrow 1$) and ^{13}CO($1 \rightarrow 0$) data offer some insight into the conditions of the molecular cloud targets. These line ratio data can also compared to the $I_{10,\rm R07}$ data. The difficulty in evaluating these results is the difference in beam sizes between the ^{12}CO($2\rightarrow1$) line (11″) and the ^{12}CO($1 \rightarrow 0$) line (14″). If the emission fills all beams, then the line ratio can be modelled using LVG analysis as was done for M33 GMCs in Wilson et al. (1997). We attempt an LVG analysis using the RADEX code (van der Tak et al. 2007). We take a typical column density of $N_{\rm CO} \sim 10^{17.7}$ cm^{-2} (assuming $N({\rm CO})/N({\rm H}_2 = 2\times10^{-4})$ and line FWHM of ~ 8 km s^{-1} representative of the sample. We adopt $N(^{12}{\rm CO})/N(^{13}{\rm CO})$=70 following Wilson et al. (1997) though they argue that LVG results are relatively insensitive to this ratio. We calculate an LVG model for two extreme conditions: (1) the emission is uniform within all the beams so the source-beam coupling is unity or (2) the emission is a point source within the beam so the intensities must be scaled by the ratio of the beam areas for comparing the lines. We model the expected line ratios ^{12}CO($2\rightarrow1$)/^{12}CO($1\rightarrow0$) and ^{13}CO($2\rightarrow1$)/^{12}CO($2\rightarrow1$) for a grid of density ($n = 10^{1.5} \rightarrow 10^{5.5}$ cm^{-3}) and temperature conditions ($T_K = 5$ K $\rightarrow$ 100 K). We find solutions where the physical conditions produce a consistent set of line ratios and label those points with the M33GMC number in Figure 3. The models have no free parameters and thus are able to replicate line ratios exactly, provided the results are sampled on the grid. Observations of more lines would enable a statistically robust determination of cloud properties. While the permitted range of conditions is broad depending on assumptions regardings source structure, we find no cloud that is inconsistent with all clouds being typical GMCs (i.e., $n \sim 10^3$ cm^{-3} and $T \sim 15$ K). While there is some concern that the conditions in the clouds may not be well suited for HCN ($1 \rightarrow 0$) emission, the line ratio studies are consistent with these objects being normal GMCs.

4 DISCUSSION

The minimal HCN emission from M33 is striking, especially compared with the active star formation from the galaxy as a whole. In particular, M33GMCs 91 and 26 highlight the deficit of HCN emission relative to CO when compared

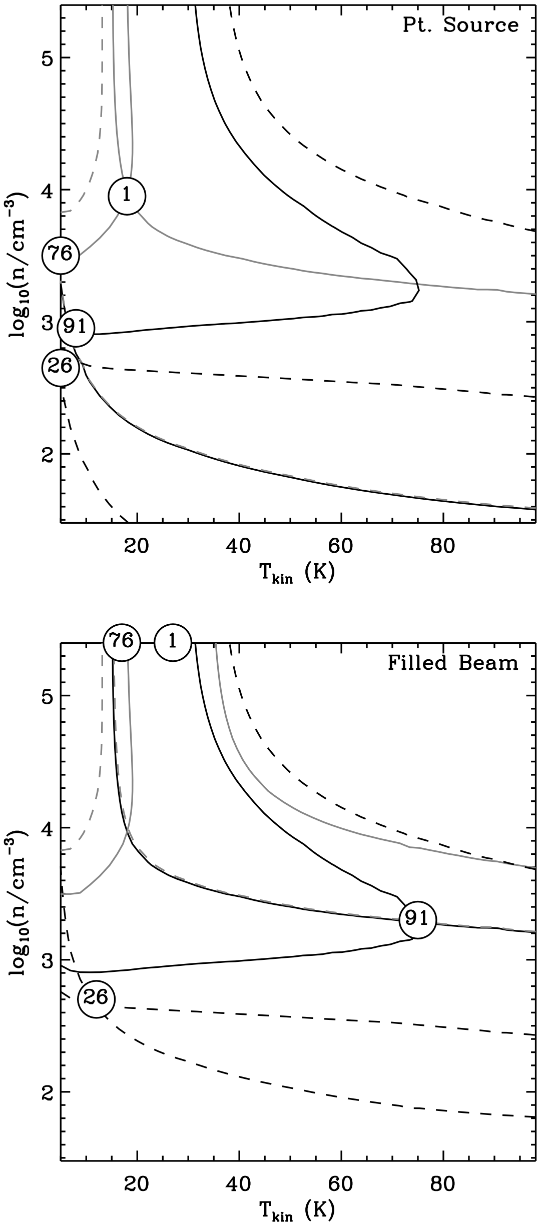

Figure 3. Large Velocity Gradient analyses of the pointings in the observation using the RADEX code applied to the ^{12}CO(2 $\rightarrow$ 1) and (1 $\rightarrow$ 0) lines and the ^{13}CO(2 $\rightarrow$ 1) line. The top and bottom panels indicate the result assuming that all the emission from the GMC targets is either a point source (top) or beam-filling (bottom). The lines are shown to indicate conditions producing a line ratio. Intersections between pairs of lines show where conditions produce both line ratios, which are labelled with the corresponding M33GMC number. Points occur at the edge of the model grid if the solution is outside the sample box.

to Milky Way clouds throughout the disk. We note that M33GMC 91 is the most massive cloud in M33. M33GMCs 1 and 76 show marginal detections consistent with the outer bounds of what is expected from Milky Way and other local galaxies. In this section, we explore possible explanations for the high CO/HCN ratios observed.

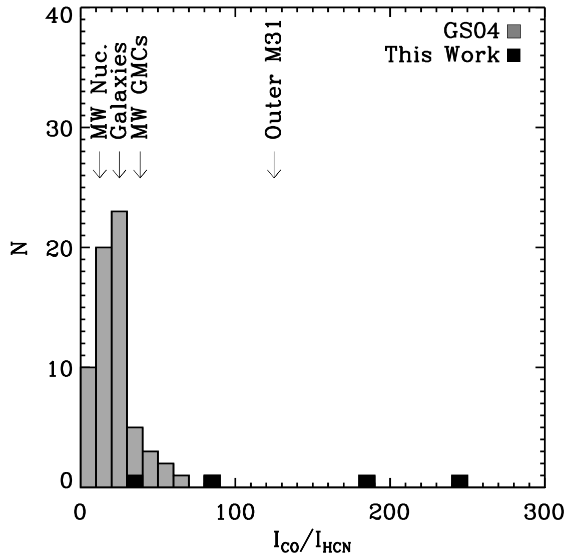

Figure 4. CO-to-HCN ratios for low-z galaxies (Gao & Solomon 2004, , grey) and for M33 pointings (black). The distribution shows that the HCN emission is anomalously weak compared to CO when viewed in the context of galaxies. The highest value of the CO-to-HCN emission is associated with the most massive GMC in M33.

The best comparable study of CO-to-HCN ratios in Local Group galaxies is the work of Brouillet et al. (2005, B05), who used the IRAM 30-m telescope to observe 16 lines of sight in M31. Their work found a radial decrease in $I_{\rm CO}/I_{\rm HCN}$ ranging from 30 to 125 at the outer limit (see Figure 4). B05 interpreted the radial variation as a reflection of a decrease in dense gas content of molecular clouds at larger galactocentric radius, consistent with the decrease seen in Helfer & Blitz (1997). However, both M31 and the Milky Way show relatively normal star formation efficiencies for their molecular gas content, in contrast with M33. Further, all of the B05 measurements are in regions with $I_{\rm CO}/I_{\rm HCN}$ and metallicity (Blair et al. 1982) similar to the Milky Way measurements.

4.1 Excitation Conditions

In this work, we have focused our analysis on the (1 $\rightarrow$ 0) lines of ^{12}CO and HCN. Following a significant number of authors, we have taken the CO emission to trace the "low-density" emission in a molecular cloud ($n \sim 10^2$ cm^{-3}), whereas the HCN line traces high density gas within the cloud. The latter statement is largely motivated by the high critical density of the transition. However, the critical density is only a rough indicator of the excitation conditions of the gas. High temperatures ($T > 50$ K) and significant radiative pumping can bring sharp departures from this "common sense." Without a full, multi-line analysis of the species, a firm interpretation is impossible (§3). However, the analysis of the physical conditions in M33 clouds suggest that these systems are analogous to GMCs found in the Milky Way (Wilson et al. 1997; Helfer & Blitz 1997), rather than active galactic nuclei where substantial concerns about the interpretation of HCN have been raised. Hence, relying on the ($1 \rightarrow 0$) lines of CO and HCN as tracers of low- and high-density gas respectively appears justified.

4.2 Metallicity and Chemical Abundances

The M33 system is substantially more metal poor (Rosolowsky & Simon 2008) with all but the central measurement in the present study occurring at lower metallicity than any point in the M31 study. The metallicity may approach solar in the inner 1 kpc (Magrini et al. 2007) which harbours M33GMC1. The similarities in pressure (see below) and the presence of significant amounts of star formation in the clouds suggests that there should be sufficient dense gas to excite HCN emission if it is present. The lower overall metallicity is also related to depletion of secondary (N) elements relative to primary elements (C,O), so HCO+ may be a more viable tracer of dense gas in low metallicity systems. Magrini et al. (2007) find a [N/O] ratio 0.3 dex lower than solar abundances across the entire galaxy. This depletion may translate directly to lower HCN/H_2 abundances.

To evaluate the effects of lower metallicity on the relative abundance of chemical species, we integrated a set of chemical models using the Nahoon code (Wakelam et al. 2004). We considered a set of eight models spanning a range from $\log[(O/H)/(O/H)_\odot] = 0.0$ to -0.4 in uniform logarithmic steps and $\log[(N/O)/(N/O)_\odot] = 0.0$ to -0.3 in uniform logarithmic steps. Solar abundances were set at the Nahoon defaults: He/H $= 0.14$, C/H $= 7.3\times10^{-5}$, N/H $= 2.14\times10^{-5}$, O/H $= 1.76 \times 10^{-4}$, Cl/H $= 4 \times 10^{-9}$, F/H $= 6.68 \times 10^{-9}$, Fe/H $= 3\times10^{-9}$, Mg/H $= 7\times10^{-9}$, Na/H $= 2\times10^{-9}$, P/H $= 3 \times 10^{-9}$, S/H $= 8 \times 10^{-8}$, Si/H $= 8 \times 10^{-9}$. We scaled the solar abundances of α-process elements to track the O abundance (C, Mg, S, Si) and all other elements to track N (Cl, F, P, Na). Grain abundance was depleted by the same factor as O. We use standard initial conditions for chemical models, including $n_{\mathrm{H2}} = 10^4$ cm^{-3} and $T = 10$ K. The models use the 2005 OSU Astrochemistry Rate compilation distributed with the Nahoon package. The rates track 4423 reactions among 452 species.

We compared the abundance of several chemical species at $t = 10^7$ years (the typical lifetime of a GMC) to evaluate the effects of depletion and low metallicity on the formation of various species, specifically HCN and CO. We find the CO abundance is a reasonable value for the solar abundance model (CO/$H_2 = 1.4 \times 10^{-4}$) and decreases roughly linearly with the decreasing metallicity. Contrary to expectations, the HCN abundance is nearly constant with decreasing metallicity (HCN/$H_2 = (1.4\pm0.1)\times10^{-9}$), as a result the CO/HCN ratio actually decreases by a factor of 2.5 going from solar to M33 abundances. These models are necessarily coarse approximations to the actual chemistry present in clouds. However, they do not indicate significant increase of the CO/HCN abundance with a decreasing N/O ratio. The ratio HCO+/HCN is also roughly constant with metallicity. While not conclusive, these models are a reminder that the abundances of individual chemical species need not track the abundances of elements of which they are composed. Hence, metallicity changes do not appear to explain the dearth of HCN in M33. Hily-Blant et al. (2010) have shown that the HCN ratio is insensitive to C/O variations in the gas, similar to the model's N/O and O/H robustness. A full treatment, including the effects of radiation (as was done for CO in Bell et al. 2006; Glover et al. 2010), is needed to validate this initial exploration.

Some authors have raised concerns about the utility of HCN as a star formation tracer, noting that AGN activity could decrease the CO/HCN ratio such that there would appear to be more dense gas than expected (e.g. Meijerink et al. 2007). We note that this is not a concern here because such effects invoke x-ray irradiation by an AGN and such effects should make HCN easier rather than more difficult to detect.

Studies of HCN formation in photodissociation regions (Young Owl et al. 2000; Boger & Sternberg 2005) suggest that HCN is readily photodissociated in translucent regions. Their work shows that HCN does not reach significant concentrations unless shielded by 4 to 8 magnitudes of visual extinction, depending on the local conditions. Given that CO forms more readily ($A_V \sim 2$), translucent clouds will show a high CO/HCN ratio. If the subsolar metallicity in M33 predicts for lower dust-to-gas ratios, then the fraction of the volume of the molecular cloud at high A_V may be significantly reduced, increasing the CO/HCN ratio. Identical reasoning is forwarded to explain the low brightness of CO in the SMC and other low metallicity systems (e.g., Israel 1997; Leroy et al. 2009, among others). Given the ample evidence for such an effect in low metallicity systems, it may hold that HCN will cease to be a good tracer of star formation at modest metallicities (e.g., $\log([O/H]) + 12 \sim 8.4$) because of dissociation effects. Further studies of the dust content of M33 are ongoing and should clarify the importance of photodissociation at regulating the CO/HCN ratio on GMC scales (Braine et al. 2010).

4.3 ISM Structure

Changes in the structure of the ISM are important at setting the CO/HCN ratio in starburst systems, where the dense gas occupies a large fraction of the ISM (Gao & Solomon 2004). This change reduces the CO/HCN ratio. It is conceivable that a similar effect is at work here. However, the molecular cloud population in M33 has been studied extensively (Wilson & Scoville 1990; Rosolowsky et al. 2003, 2007), reaching the conclusion that the individual clouds have similar macroscopic properties as those found in the Milky Way and M31, including turbulent line widths and average densities.

The properties of these clouds are linked to the galactic environment via pressure. Helfer & Blitz (1997) demonstrate that HCN-to-CO ratio correlates with the disk pressure in the ISM at the galactocentric radius of the objects observed: $I_{\mathrm{HCN}}/I_{\mathrm{CO}} \propto P^{0.19\pm0.04}$. Higher pressures in the galactic environment would cause GMCs to have correspondingly higher pressure to maintain their distinction from the remainder of the ISM. As seen in Table 2, the disk pressure values are comparable to the Milky Way disk values, implying these GMCs do not fall on the scalings of Helfer & Blitz (1997). Following their scaling, we predict $I_{\mathrm{CO}}/I_{\mathrm{HCN}} \sim 30 - 50$ in these clouds which is only consistent with a marginal detection from M33GMC 1. Thus, it seems unlikely that the dense gas content of these clouds would be significantly lower than those in the other local group disk systems. This is because the dense gas fraction of clouds has a tight link between the average density and amount of turbulent driving (e.g., Padoan & Nordlund 2002; Krumholz & Thompson 2007).

4.4 Infrared Luminosity and Evolution

The motivation for studying HCN in M33 comes from the intimate link between star formation (as implied by infrared emission) and HCN emission in galaxies. In Figure 5, we consider the infrared and HCN emission in the context of other studies.

The targets in M33 are comparable to high luminosity star forming regions in the Milky Way. While they appear significantly above the mean ratio defined by galaxies ($L_{\rm IR}/L_{\rm HCN}=800$), the lines-of-sight appear consistent with the upper envelope of values derived for the Milky Way regions. We note that the observed clouds have substantial masses ($>10^5~M_{\odot}$, Rosolowsky et al. 2007) and their infrared luminosities are well above the threshold above which the HCN-to-IR ratio saturates at its constant ratio (Figure 5, Wu et al. 2010). Specifically, M33GMC 1 and 76 have bright, discrete HII regions located within the IRAM beam, in addition to being strong CO emitters. Although Wu et al. (2010) have argued for a constant $L_{\rm IR}/L_{\rm HCN}$ ratio for $L_{\rm IR}>10^{4.5}~L_{\odot}$, the addition of the M33 points to the upper envelope of the trend suggest a continuation to higher ratios at larger luminosities. Hence, the remarkably consistent values for the IR-to-HCN ratio seen in galaxies may actually derive from consistent sampling from a population with a changing ratio.

The relationship between star formation and dense molecular gas emission is not universal. Indeed, Gao et al. (2007) found that four high redshift galaxies ($z=1.0\rightarrow 2.8$) show $L_{\rm HCN}/\dot{M}_{\star}$ that is a factor of 2 lower than the result established in the local population and several non-detections of HCN suggest a cosmological evolution of the star formation efficiency of dense gas. While the GMCs in M33 do not have star formation efficiencies as high as observed in some high redshift systems, the results are consistent with the star formation efficiency of HCN-emitting gas being comparable to or larger than that observed in high redshift systems.

This study observes individual GMCs whereas the other studies focus on galaxies (Gao & Solomon 2004; Gao et al. 2007) or individual star forming regions (Wu et al. 2005). Thus, the evolution of GMCs via cloud evolution and star formation processes may cause scatter in the interpretation of star formation efficiency. We have selected GMCs such that $L_{\rm IR}/L_{\rm CO}$ spans a large range. While not conclusive, it is suggestive that the two marginal detections showing the lowest $I_{\rm CO}/I_{\rm HCN}$ ratios are also the most infrared luminous. The lack of dense gas in M33GMCs 91 and 26 may indicate these are younger, less evolved systems. The factor-of-ten range in star formation rates derived from the IR + Hα emission suggests that variations in evolutionary stages may indeed be responsible for the low levels of HCN emission seen from M33GMCs 91 and 26. Thus, a possible explanation for the highest values of CO-to-HCN may be that these clouds are young and have not formed significant fractions of high density gas.

5 CONCLUSIONS

In summary, we have searched for and failed to find significant HCN emission from GMCs in M33. The HCN observations are sufficiently sensitive that the HCN should be easily detected ($>20\sigma_{rms}$) if the emission were present at the levels expected based off either CO or star formation observations in our Galaxy and others (Helfer & Blitz 1997; Gao & Solomon 2004; Wu et al. 2005). Two of the four lines of sight that we observed show a marginal detection of HCN emission and these two targets are bright infrared sources in the galaxy. Using naïve chemical models, we explored the effects of the low metallicity and N/O depletion in M33 on the CO/HCN ratio. Despite depletion of N/O, the CO/HCN ratio is predicted to be lower in M33 than in the Milky Way. Since HCN only forms at high extinction relative to C/O, the low metallicity of the galaxy may result in reduced dust shielding and thus more molecular gas exposed to dissociating radiation. Even though the ratio of $L_{\rm IR}/L_{\rm HCN}$ is a factor of six larger than the mean for galaxies, it is nonetheless consistent with comparable systems in the Milky Way. The M33 targets appear most distinct in their CO-to-HCN ratios rather than in their infrared luminosities. This suggests that the low levels of HCN emission likely reflect a smaller fraction of dense, shielded gas in these clouds rather than a systematic effect. Having considered chemical and structural variations, the observed discrepancies seem most likely to be the result of either reduced extinction or cloud evolution effects. A larger sample of GMC-based observations and a clearer understanding of the dust properties in M33 are needed to clarify these results.

ER and JP are supported by an NSF AAP Fellowship (AST-0502605). ER is further supported by a Discovery Grant from NSERC of Canada. YG's research is partially supported by China NSF Innovation Team (#10621303), Distinguished Young Scholars (#10425313), 973 of the Ministry of Science & Technology and Chinese Academy of Sciences' Hundred Talent Program. We are grateful for the comments of an anonymous referee, in particular regarding the importance of UV dissociation at regulating the CO/HCN abundance.

REFERENCES

Bell T. A., Roueff E., Viti S., Williams D. A., 2006, MNRAS, 371, 1865

Bigiel F., Leroy A., Walter F., Brinks E., de Blok W. J. G., Madore B., Thornley M. D., 2008, AJ, 136, 2846

Blair W. P., Kirshner R. P., Chevalier R. A., 1982, ApJ, 254, 50

Blitz L., Rosolowsky E., 2006, ApJ, 650, 933

Boger G. I., Sternberg A., 2005, ApJ, 632, 302

Braine J., Gratier P., Kramer C., Xilouris E. M., Rosolowsky E., Buchbender C., Boquien M., Calzetti D., Quintana-Lacaci G., Tabatabaei F., Verley S., Israel F., van der Tak F., Aalto S., Combes F., Garcia-Burillo S., Gonzalez M., Henkel C., Koribalski B., Mookerjea B., Roellig M., Schuster K. F., Relaño M., Bertoldi F., van der Werf P., Wiedner M., 2010, A&A, 518, L69+

Brouillet N., Muller S., Herpin F., Braine J., Jacq T., 2005, A&A, 429, 153

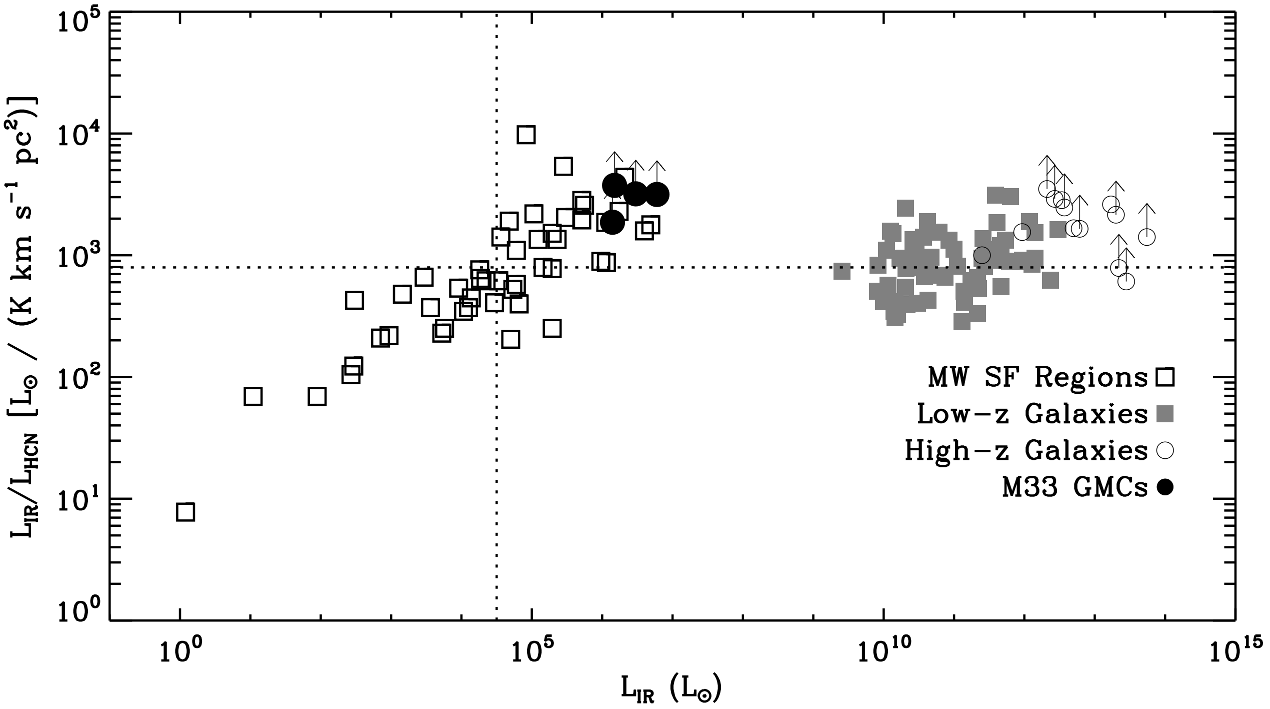

Figure 5. Comparison of M33 GMCs to literature data for $L_{\rm IR}$ and $L_{\rm HCN}$. Milky Way star forming region data are from Wu et al. (2010); Low-z galaxies are from Gao & Solomon (2004); high-z galaxies are from Gao et al. (2007). The horizontal line at a ratio of $L_{\rm IR}/L_{\rm HCN} = 800$ is the mean ratio for regions with $L_{\rm IR} > 3 \times 10^4$ $L_\odot$ forwarded by Wu et al. (2010). The vertical line at $L = 10^{4.5}$ $L_\odot$ is attributed to the threshold below which the IMF is not fully sampled in the system. The M33 GMCs are consistent with the upper end of the galactic population, but the regions are significantly above the mean ratio.

Dale D. A., Helou G., 2002, ApJ, 576, 159

Freedman W. L., Madore B. F., Gibson B. K., Ferrarese L., Kelson D. D., Sakai S., Mould J. R., Kennicutt Jr. R. C., Ford H. C., Graham J. A., Huchra J. P., Hughes S. M. G., Illingworth G. D., Macri L. M., Stetson P. B., 2001, ApJ, 553, 47

Gao Y., Carilli C. L., Solomon P. M., Vanden Bout P. A., 2007, ApJ, 660, L93

Gao Y., Solomon P. M., 2004, ApJ, 606, 271

Gardan E., Braine J., Schuster K. F., Brouillet N., Sievers A., 2007, A&A, 473, 91

Glover S. C. O., Federrath C., Mac Low M., Klessen R. S., 2010, MNRAS, 404, 2

Helfer T. T., Blitz L., 1997, ApJ, 478, 233

Heyer M. H., Corbelli E., Schneider S. E., Young J. S., 2004, ApJ, 602, 723

Hily-Blant P., Walmsley M., Pineau Des Forêts G., Flower D., 2010, A&A, 513, A41+

Hinz J. L., Rieke G. H., Gordon K. D., Pérez-González P. G., Engelbracht C. W., Alonso-Herrero A., Morrison J. E., Misselt K., Hines D. C., Gehrz R. D., Polomski E., Woodward C. E., Humphreys R. M., Regan M. W., Rho J., Beeman J. W., Haller E. E., 2004, ApJS, 154, 259

Israel F. P., 1997, A&A, 328, 471

Kennicutt R. C., 1998, ApJ, 498, 541

Kennicutt Jr. R. C., 2007, ApJ, 671, 333

Kennicutt Jr. R. C., Calzetti D., Walter F., Helou G., Hollenbach D. J., Armus L., Bendo G., Dale D. A., Draine B. T., Engelbracht C. W., Gordon K. D., Prescott M. K. M., Regan M. W., Thornley M. D., Bot C., Brinks E., de Blok E., de Mello D., Meyer M., Moustakas J., Murphy E. J., Sheth K., Smith J. D. T., 2007, ApJ, 671, 333

Krumholz M. R., Thompson T. A., 2007, ApJ, 669, 289

Lada E. A., 1992, ApJ, 393, L25

Leroy A. K., Bolatto A., Bot C., Engelbracht C. W., Gordon K., Israel F. P., Rubio M., Sandstrom K., Stanimirović S., 2009, ApJ, 702, 352

Magrini L., Vílchez J. M., Mampaso A., Corradi R. L. M., Leisy P., 2007, A&A, 470, 865

Massey P., McNeill R. T., Olsen K. A. G., Hodge P. W., Blaha C., Jacoby G. H., Smith R. C., Strong S. B., 2007, AJ, 134, 2474

Matthews L. D., Gao Y., 2001, ApJ, 549, L191

Meijerink R., Spaans M., Israel F. P., 2007, A&A, 461, 793

Narayanan D., Cox T. J., Shirley Y., Davé R., Hernquist L., Walker C. K., 2008, ApJ, 684, 996

Padoan P., Nordlund Å., 2002, ApJ, 576, 870

Pineda J. E., Caselli P., Goodman A. A., 2008, ApJ, accepted (arXiv:0802:0708)

Polomski E., Gehrz R. D., Woodward C. E., Humphreys R. M., Boyer M., Brandl B. R., van Loon J., Fazio G., Willner S. P., Barmby P., Ashby M., Pahre M., Rieke G., Gordon K., Hinz J., Engelbracht C., Alonso-Herrero A., Misselt K., Pérez-González P. G., Roellig T., 2006, in Armus L., Reach W. T., eds, Astronomical Society of the Pacific Conference Series Vol. 357 of Astronomical Society of the Pacific Conference Series, Multi-Epoch Imaging and

Spectroscopy of M33. pp 196–+

Rosolowsky E., Keto E., Matsushita S., Willner S. P., 2007, ApJ, 661, 830

Rosolowsky E., Simon J. D., 2008, ApJ, 675, 1213

Rosolowsky E. W., Plambeck R., Engargiola G., Blitz L., 2003, ApJ, 599, 258

Shirley Y. L., Wu J., Shane Bussmann R., Wootten A., 2008, in Beuther H., Linz H., Henning T., eds, Massive Star Formation: Observations Confront Theory Vol. 387 of Astronomical Society of the Pacific Conference Series, The Properties of Dense Molecular Gas in the Milky Way and Galaxies. pp 401–+

Tabatabaei F. S., Beck R., Krause M., Berkhuijsen E. M., Gehrz R., Gordon K. D., Hinz J. L., Humphreys R., McQuinn K., Polomski E., Rieke G. H., Woodward C. E., 2007, A&A, 466, 509

van der Tak F. F. S., Black J. H., Schöier F. L., Jansen D. J., van Dishoeck E. F., 2007, A&A, 468, 627

Wakelam V., Caselli P., Ceccarelli C., Herbst E., Castets A., 2004, A&A, 422, 159

Wilson C. D., Scoville N., 1990, ApJ, 363, 435

Wilson C. D., Walker C. E., Thornley M. D., 1997, ApJ, 483, 210

Wong T., Blitz L., 2002, ApJ, 569, 157

Wu J., Evans N. J., Shirley Y. L., Knez C., 2010, ApJS, 188, 313

Wu J., Evans II N. J., Gao Y., Solomon P. M., Shirley Y. L., Vanden Bout P. A., 2005, ApJ, 635, L173

Young Owl R. C., Meixner M. M., Wolfire M., Tielens A. G. G. M., Tauber J., 2000, ApJ, 540, 886